PAPER

Manipulating interlayer morphology in electrospun bipolar membranes: a key to overcoming the trade-off between perm-selectivity and resistance

Tao Wang, [iD] Nadia Boulif, Zandrie Borneman and Kitty Nijmeijer*

Bipolar membranes (BPMs) face a fundamental performance trade-off between low resistance and high perm-selectivity. Here, we report a breakthrough strategy using scalable electrospinning and precisely controlled hot-pressing to fabricate electrospun BPMs that simultaneously achieve both. A phytic acid and Fe^{3+} complex was utilized for the first time as a water dissociation catalyst. By controlling the number of electrospun mats in hot-pressing, we successfully developed electrospun BPMs with tunable thicknesses ranging from 40 to 90 μm. Critically, we demonstrate that the perm-selectivity and conductance both increase as membrane thickness decreases. Electrochemical impedance spectroscopy reveals that while ohmic resistance decreases with thickness, water dissociation resistance dominates the overall resistance by two orders of magnitude. Mechanistic insight was gained by systematically varying the hot-pressing force and applying selective pre-hot-pressing to the cation exchange layer (CEL), interfacial layer (IL), or anion exchange layer (AEL). This shows that the penetration of the AEL into the IL impedes proton crossover, thereby increasing the perm-selectivity of the BPM. Significantly, while a lower number of electrospun mats in hot-pressing results in an enhanced penetration of the AEL into the IL, the thinner electrospun BPM exhibited both lower resistance and higher perm-selectivity. Guided by this mechanism, we fabricated a BPM by hot-pressing only one AEL and one highly selective and catalytic CEL, exhibiting a voltage drop value of 1.0 V at 100 mA cm^{-2} and a perm-selectivity of 95%. This work offers valuable insights into the structural design of electrospun BPMs, overcoming the trade-off between resistance and perm-selectivity.

1. Introduction

Renewable energy conversion and energy storage technologies, including water electrolysis, CO_2 conversion, resource recovery, flow batteries, and fuel cells, are the cornerstone of a sustainable society.[1-3] As a critical component of these electrochemical technologies, bipolar membranes (BPMs) have gained increasing attention.[4] The typical structure of a BPM comprises of an interfacial layer (IL) that contains a catalyst sandwiched between a negatively charged cation exchange layer (CEL) and a positively charged anion exchange layer (AEL).[5] In reverse bias, water dissociation occurs at the IL, while in forward bias, H^+ and OH^- ions migrate towards the IL, recombining to form water molecules. Benefiting from the second Wien effect and the catalysed protonation–deprotonation mechanism, the water dissociation rate of BPMs in reverse bias is 10^4 to 10^6 times higher than that observed in bulk solution, making it a highly promising technique for water electrolysis.[6] BPMs efficiently separate reactants and products between the anode and cathode. The fixed ionic charges in the CEL and AEL ionomers

limit the crossover of co-ions *via* electrostatic forces. This limited crossover of co-ions ensures a stable pH environment at the electrodes during reactions.[3]

From the perspective of practical applications, BPMs should ideally exhibit high water dissociation efficiency, low resistance, high selectivity, and stable performance at operational current densities. However, the high resistance of BPMs and the inadequate water diffusion result in limiting currents in reverse and forward bias that are lower than 100 and 5 mA cm^{-2}, respectively.[7] To minimize the resistance of BPMs and enhance water transport, a common strategy is to increase the ion exchange capacity (IEC) of the polymers forming the BPMs.[8] However, a high IEC typically accompanies enhanced water adsorption, leading to significant swelling of nanochannels in the membrane and ultimately, a decline in membrane perm-selectivity. As theoretically Donnan exclusion is not directly dependent on membrane thickness, whereas the relationship between conductance and thickness is linear, reducing the membrane thickness provides an opportunity to decrease resistance without compromising the selectivity.[5]

The manipulation of BPM thickness was first demonstrated by Wilhelm *et al.*, where BPMs with an asymmetric thickness of CEL and AEL were employed to decrease the co-ion leakage at

Membrane Materials & Processes, Technology University of Eindhoven, The Netherlands. E-mail: D.C.Nijmeijer@tue.nl

2274 | *J. Mater. Chem. A*, 2026, **14**, 2274–2283

This journal is © The Royal Society of Chemistry 2026

the cost of limited water diffusion.[9–11] In recent years, significant research efforts have been directed toward reducing the thickness of BPMs to explore their applications at high current densities. The modelling work from Bui et al. highlights that decreasing AEL thickness is more effective than decreasing the CEL thickness due to the higher transport coefficient for H^+ compared to OH^-.[12] Nevertheless, Oener et al. have the opinion that thinning the AEL poses a risk to stability as the oxidizing anode potentials on the AEL side can result in the degradation of membranes. To overcome this, they did the contrary and developed a BPM with a 2 μm CEL and a 50 μm AEL, achieving a current density of 3400 mA cm^{-2} with a voltage drop of only 4 V during water electrolysis.[13] However, Zabolotskii et al. reported contrasting findings. Their electrochemical impedance spectroscopy (EIS) analysis indicated that reducing the CEL thickness has minimal influence on decreasing the ohmic resistance of BPMs but may compromise perm-selectivity.[14] Furthermore, the EIS results also showed that the contribution of ohmic resistance to the total resistance of the BPM was less than 5%, suggesting that reducing water dissociation resistance, equivalently enhancing the catalytic efficiency of the catalyst, is more crucial than reducing the thickness of the BPM. As discussed above, a significant gap persists in the literature concerning a comprehensive and systematic exploration of the impacts of CEL, IL, and AEL thickness on both BPM resistance and selectivity. To properly address this, precise control over the thicknesses of the CEL, IL, and AEL is a prerequisite.

Electrospinning, a simple and cost-effective technique for creating nanofiber mats with a high surface-to-volume ratio, has proven to be effective in developing BPMs. Moreover, the nanofibers provide sufficient surface area suitable for embedding water dissociation catalysts, such as nanosized silica MCM-41,[15] metal–organic frameworks (MOFs),[16] graphene oxide,[17] poly(4-vinylpyrrolidine) (P4VP),[18] montmorillonite,[19] and weak polyelectrolytes: polyethyleneimine (PEI) and poly(acrylic acid) (PAA).[20] To integrate CEL, IL, and AEL, hot-pressing is commonly employed, transforming porous nanofiber mats into dense ion exchange membranes.[17,20] Notably, this method allows feasible and precise control over the thickness of CEL and AEL by adjusting the number of electrospun mats in hot-pressing. Furthermore, the three-dimensional entangled structure has been shown to enhance the stability of the IL, increase the catalytic site density, and facilitate transport pathways for H_2O, H^+, and OH^-.[21] However, to date, no research has been conducted systematically, exploring the effects of the thicknesses of CEL, IL, and AEL in electrospun BPMs while electrospinning offers an excellent opportunity to do so. Moreover, the role of the catalyst coated on the IL, particularly its influence on the perm-selectivity of BPMs, has been largely overlooked. Previous studies conducted by our research group have indicated that polyelectrolyte multilayers coated on the IL not only function as a catalyst but also improve the perm-selectivity of BPMs.[19,20] Consistent findings have been reported by Al-Dhubhani et al.[22] and Hohenadel et al.,[23] highlighting that with identical CEL and AEL, the perm-selectivity of a BPM is significantly influenced by the characteristics of the IL region, such as the types of catalyst and its thickness. Nevertheless,

despite the importance of the IL, further investigation into the mechanism of this enhanced perm-selectivity of the electrospun BPMs remains lacking.

In this work, electrospun BPMs with systematically varied thicknesses are fabricated by controlling the number of CEL and AEL electrospun mats in hot-pressing. Due to the excellent catalytic ability of phosphate groups and Fe^{3+} ions for water dissociation,[24,25] and also the good stability of transition metal phosphide in both acid and base,[26] for the first time, a phytic acid and Fe^{3+} complex is formed on the surface of nanofibers to work as a catalyst for water dissociation. The effects of CEL and AEL thickness on the performance of BPMs are systematically investigated by electrochemical measurements, including current–voltage ($i–v$) curves, perm-selectivity analysis, and EIS. Tailored mechanical force during hot-pressing is employed to investigate interlayer interpenetration among the CEL, IL, and AEL. This work not only establishes a validated methodology for fabricating high-performance BPMs but also offers valuable insights into the design of electrospun BPMs with a focus on the catalyst and the often-overlooked interlayer morphology between the CEL, IL, and AEL.

2. Results and discussion

2.1. Phytic acid–Fe^{3+} complex as a catalyst for water dissociation

Both experimental and modelling studies reported that the water dissociation catalyst inside the IL of BPM significantly influences the water dissociation efficiency.[5,6,27] In this work, a complex formed by phytic acid and Fe^{3+} was coated onto the surface of the sulfonated poly(ether ether ketone) (SPEEK) electrospun mat. As illustrated in Fig. 1a, through the Layer-by-Layer (LbL) assembly technique, positively charged PEI was first coated on SPEEK, and the phytic acid–Fe^{3+} complex was formed on top of it. Fig. 1b shows the morphologies of the electrospun mats of (i) pristine SPEEK, (ii) SPEEK coated with the phytic acid–Fe^{3+} complex, and (iii) pristine FAA-3, respectively, all of which exhibit micro-sized fiber structures. Notably, the fiber diameter of the SPEEK coated with the phytic acid–Fe^{3+} complex (ii) is slightly larger than that of pristine SPEEK (i), which can be attributed to the irreversible swelling during the coating of the phytic acid–Fe^{3+} complex. The successful coating of the phytic acid–Fe^{3+} complex is evidenced by the energy-dispersive X-ray spectroscopy (EDS) results in Fig. S1, where the presence of iron and phosphorus elements on the surface of the coated SPEEK was detected. Furthermore, water contact angle measurements (Fig. S2) confirm the enhanced hydrophilicity of the coated SPEEK electrospun mat, which is consistent with the findings in the work of Li et al.[28] This hydrophilic coating enhances water transport towards the catalysts in the electrospun BPM.[29] Subsequently, negatively charged pristine SPEEK, SPEEK coated with the phytic acid–Fe^{3+} complex, and positively charged FAA-3 were hot-pressed together to form a BPM (Fig. 1c). During this hot-pressing process, manipulating the number of SPEEK and FAA-3 electrospun mats allowed feasible regulation of the BPM structure (the thicknesses of the CEL and AEL). The BPMs are denoted as "x–y–z", where "x", "y", and "z"

This journal is © The Royal Society of Chemistry 2026

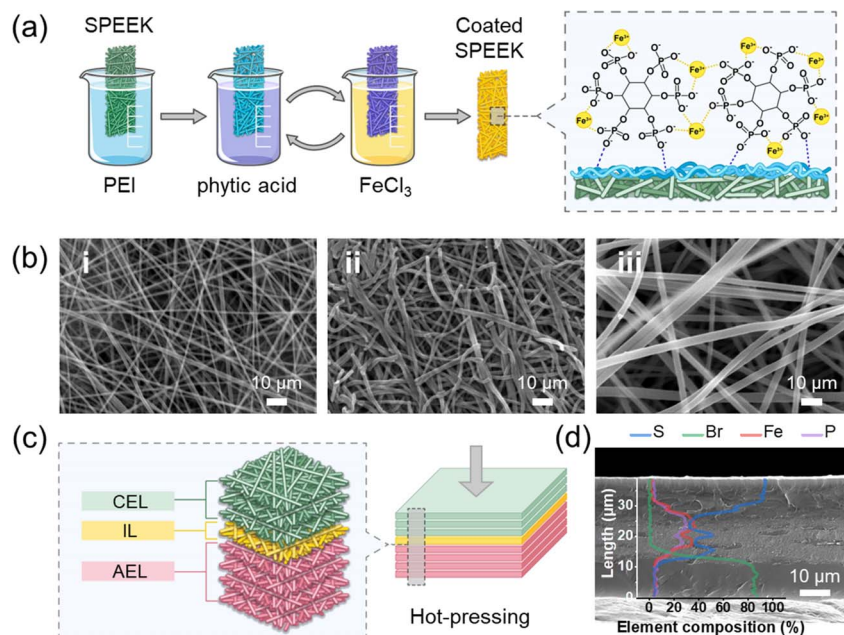*J. Mater. Chem. A*, 2026, **14**, 2274–2283 | **2275**

Fig. 1 The fabrication of the electrospun BPMs: (a) Layer-by-Layer (LbL) coating of polyethyleneimine (PEI), phytic acid, and FeCl$_3$ on a sulfonated poly(ether ether ketone) (SPEEK) electrospun mat; (b) surface morphologies of (i) SPEEK electrospun mat, (ii) SPEEK coated with the phytic acid–Fe^{3+} complex, and (iii) FAA-3 electrospun mat before hot-pressing; (c) hot-pressing of multiple electrospun mats to obtain electrospun BPMs. The thickness of the BPM was controlled by varying the number of CELs and AELs; (d) the morphology and elemental composition of the cross-section of the BPM (2–1–1) after hot-pressing.

represent the number of SPEEK electrospun mats (CEL), LbL-coated electrospun mat (IL), and FAA-3 electrospun mats (AEL) in hot-pressing, respectively. As shown in Fig. 1d, the cross-section image of the BPM (2–1–1) exhibits a dense structure with a well-defined junction enriched in iron and phosphorus, confirming the successful incorporation of the phytic acid–Fe^{3+} complex into the IL of the BPM.

To verify the catalytic ability of the phytic acid–Fe^{3+} complex, Fig. 2 presents a comparison among a BPM without catalyst (3–0–2), a BPM with an IL coated with only PEI (2–1–1-PEI), and a BPM with an IL coated with the PEI–phytic acid–Fe^{3+} complex (2–1–1). As exhibited in Fig. 2a, different from the BPM without a catalyst (3–0–2) and the BPM with only PEI coating (2–1–2-PEI), a clear distinction is observed between the CEL, IL, and AEL when the phytic acid–Fe^{3+} complex is coated (2–1–2). Fig. 2b and c show the i–v curves and perm-selectivities, respectively. At a current density of 10 mA cm^{-2}, the voltage across the BPM without coating (3–0–2) is significantly higher than that of the BPM coated with PEI (2–1–2-PEI) and phytic acid–Fe^{3+} (2–1–2). Although the PEI coating can also function as a catalyst for water dissociation,[20] the catalytic efficiency of the phytic acid–Fe^{3+} complex is much higher than that of PEI only. Meanwhile, compared to the BPM without a catalyst (3–0–2), the BPM with phytic acid–Fe^{3+} (2–1–2) coating demonstrates a reduced first limiting current density and enhanced perm-selectivity, suggesting that the phytic acid–Fe^{3+} complex not only serves as a catalyst but also improves the selectivity of the BPM. Further discussion on the origin of this enhanced perm-selectivity is given in the following sections.

2.2. The effect of thickness revealed by tuning the layer number of the CEL and AEL

As noted, the thickness of the CEL and AEL was controlled by adjusting the number of SPEEK and FAA-3 electrospun mats in the BPM assembly. The number of the CELs and AELs was varied from 1 to 4 for each, while the number of the IL was fixed at 1. Fig. S3a shows the cross-sectional morphologies of the BPMs with varied numbers of CELs and AELs. As quantified using a micrometer and summarized in Fig. S3b, the BPM thickness can be controlled within a range of 40 to 90 μm. Furthermore, the number of FAA-3 electrospun mats exhibits a more pronounced influence on the BPM thickness than the number of SPEEK electrospun mats (Fig. S3c). This difference stems from the greater compressibility of the SPEEK electrospun mats during hot-pressing compared to the FAA-3 mats. This is evidenced by the densities of BPMs with the same total layer number presented in Fig. S3d: as the number of SPEEK layers (CEL) increases from 1 to 4 accompanied by a decrease in the number of AELs from 4 to 1, the density of the BPM after hot-pressing rises from 17.5 g cm^{-3} to 19.4 g cm^{-3}, highlighting the distinct compression behaviors of the two polymer materials.

This differential contribution of the CEL and AEL to thickness is also reflected in the i–v curves. As presented in Fig. S4, when the number of CELs is fixed, the voltage at 10 mA cm^{-2} rises with an increase in the number of AELs. Conversely, no clear trend is discernible when the number of AELs is fixed (Fig. S5). Given that the thickness of the BPMs varies with the number of layers, to ensure a fair comparison, the voltages for the different BPMs at 10 mA cm^{-2} are summarized and plotted
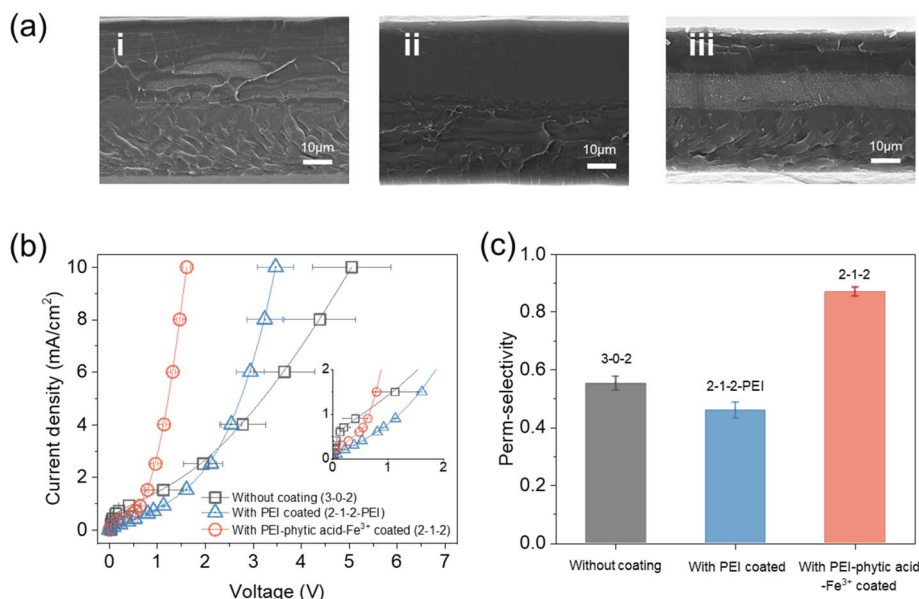
2276 | J. Mater. Chem. A, 2026, **14**, 2274–2283

This journal is © The Royal Society of Chemistry 2026

Fig. 2 The comparison of the BPM without a catalyst (3−0−2), BPM with an IL coated with only PEI (2−1−2-PEI), and BPM with an IL coated with the PEI−phytic acid−Fe^{3+} complex (2−1−2): (a) cross-section morphologies of BPMs: (i) 3−0−2, (ii) 2−1−2-PEI, and (iii) 2−1−2. The CEL is on the top of three SEM images; (b) $i−v$ curves; the inset represents a zoomed-in view of the $i−v$ curves, focusing on the voltage from 0 to 2 V and the current density from 0 to 2 mA cm^2; (c) perm-selectivities.

against the corresponding BPM thickness in Fig. 3a. A clear trend can be observed: as the thickness decreases, the voltage at 10 mA cm^{-2} also declines, indicating a reduction in the overall resistance of the BPM. To further determine the contribution of the decreased thickness to the decline in membrane resistance, EIS measurements were performed (Nyquist plots shown in Fig.

S6). As illustrated in Fig. 3b, the ohmic area resistance follows the same trend as the voltage at 10 mA cm^{-2} in Fig. 3a, decreasing as the membrane thickness reduces. This confirms the effectiveness of decreasing the ohmic area resistance of a BPM by reducing its thickness. However, it is important to note that the water dissociation resistance is two orders of
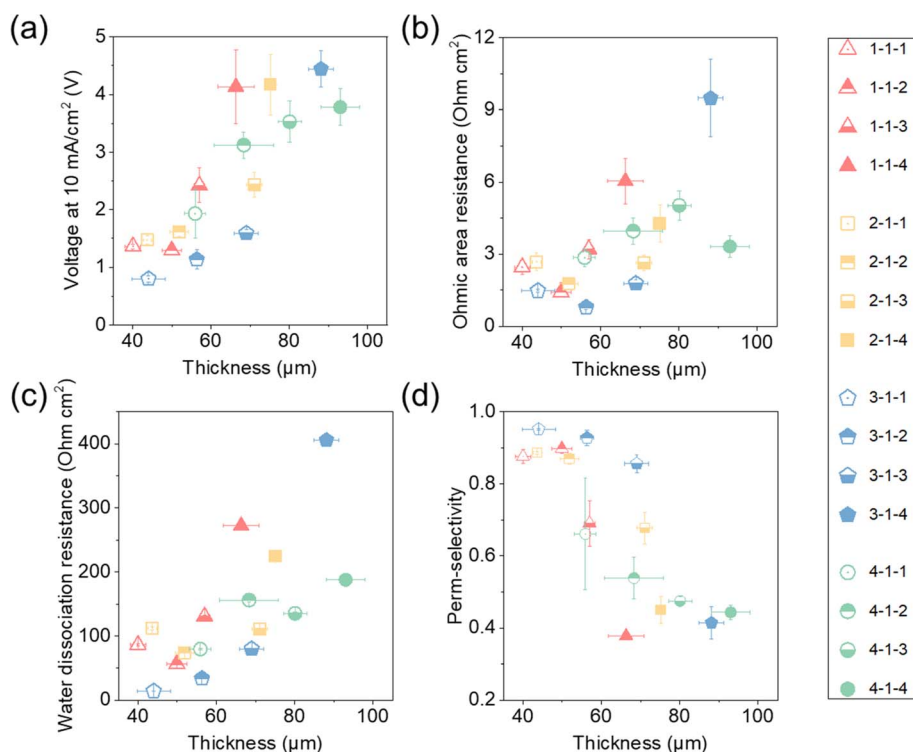

Fig. 3 Performances of BPMs with tunable CEL and AEL thicknesses: (a) voltages across the BPMs at 10 mA cm^2; (b) ohmic area resistances; (c) water dissociation resistances; (d) perm-selectivities.

This journal is © The Royal Society of Chemistry 2026

J. Mater. Chem. A, 2026, **14**, 2274–2283 | **2277**

magnitude higher than the ohmic area resistance (Fig. 3c). A similar result was also reported by Melnikov *et al.*, who showed that the contribution of ohmic resistance to the total resistance of a BPM is less than 5%.[14] Since the water dissociation overpotential is determined by the catalyst in the IL, this shows that the catalyst in the IL has a substantial impact on the overall resistance of the BPM but that membrane thickness still plays an important role. Furthermore, in Fig. 3c, the water dissociation resistance also decreases with reduced BPM thickness. Considering that for different BPMs, the same IL was employed and the hot-pressing force was fixed at 200 kN, the difference in water dissociation resistance suggests the number of electrospun mats affects the state of the catalyst in the IL. Although the hot-pressing force was constant, increasing the number of electrospun mats introduces more interfaces within the CEL (SPEEK|SPEEK) and AEL (FAA-3|FAA-3). This makes the critical CEL|IL|AEL interfaces less dense, thereby influencing the states of the catalyst on the IL. However, further investigation of the effect of hot-pressing force is needed.

Fig. 3d illustrates the perm-selectivities of all the fabricated BPMs. Intriguingly, the perm-selectivity improves as the structure of the BPM becomes thinner, which is contrary to what has been reported in the literature.[5] The limiting current density, a parameter used to assess the co-ion crossover within BPM,[30] also displays this trend in Fig. S7: it diminishes with an increase in the number of CEL and AEL electrospun mats. These findings demonstrate that our electrospun BPMs hold the potential to overcome the trade-off between low resistance and high selectivity. Even so, the exact underlying mechanism remains only partly understood. Theoretically, the selectivity of ion exchange membranes primarily relies on charge exclusion (Donnan effect), which is independent of membrane thickness.[31] However, it has been reported that when the thickness of ion exchange membranes drops below 20 μm, the thin membrane structure leads to increased diffusive fluxes, resulting in higher co-ion flux through the membrane.[32] To exclude the influence of thickness on the perm-selectivity of ion exchange membranes, varying numbers of CEL, IL, and AEL samples were hot-pressed individually. As shown in Fig. S8, increasing the number of electrospun mats from 1 to 2 enhances the perm-selectivities of both the CEL and AEL. Nevertheless, when more than two electrospun mats are hot-pressed, no significant improvement in perm-selectivity is observed. This aligns with the literature indicating that ion exchange membrane perm-selectivity becomes thickness-independent beyond a certain thickness threshold.[32] Consequently, increasing the number of electrospun mats provides no significant benefit to the perm-selectivity of monopolar ion exchange layers, as reported previously.[10]

Another noteworthy phenomenon in Fig. S8 is the higher perm-selectivity of the individually hot-pressed IL compared to the CEL or AEL. This indicates that the catalyst-coated IL contributes more to the enhanced perm-selectivity than the CEL and AEL, which is also recognized in previous studies.[19,20] Furthermore, this provides a possible explanation for achieving high perm-selectivity at low BPM thickness. As discussed above, fewer electrospun mats result in denser CEL|IL|AEL interfaces. As a result, the thinner BPM has a denser IL inside, exhibiting

higher perm-selectivity. Since the hot-pressing process plays an important role on both catalyst state and perm-selectivity, the effect of force applied during hot-pressing is further investigated in the next section.

2.3.   The effect of hot-pressing force on BPM performance

To investigate the effect of the force applied during hot-pressing on the performance of the BPM, BPMs composed of 2 CELs, 1 IL, and 2 AELs were hot-pressed under a force ranging from 200 kN to 300 kN (200 kN, 250 kN, and 300 kN). As shown in Fig. 4a, the decrease in the overall thickness is negligible when a higher force of hot-pressing is applied. Therefore, the effect of membrane thickness can be excluded from the subsequent discussion. As the i–v curves show in Fig. 4b, the voltage at 10 mA cm^{-2} decreases with an increase in hot-pressing force, suggesting that the overall resistance of the BPM reduces at a higher hot-pressing force. Fig. 4d summarizes the results of ohmic area resistance, depletion thickness, and water dissociation area resistance extracted from the EIS analysis (Fig. S9). The depletion layer thickness was calculated following the literature,[20] and a thinner depletion layer is preferred, signifying a faster proton and hydroxide ion production rate at the junction. With the increase in hot-pressing force from 200 kN to 300 kN, the change in ohmic resistance is negligible, whereas substantial decreases in water dissociation resistance, from 73.8 to 40.8 ohm cm^2, and depletion thickness, from 33.4 to 18.2 nm, can be observed. These results point out that the high force during hot-pressing enhances the water dissociation efficiency of the catalysts immobilized on the IL. This also accounts for the lower water dissociation resistance with a thinner membrane structure observed in Fig. 3c, as fewer electrospun mats result in a denser structure of the IL. However, it has been reported in the literature that a high surface area of the catalyst region is preferred for water dissociation, as it provides more reactive sites for water dissociation.[33,34] Therefore, a denser IL structure is expected to increase the water dissociation resistance. Considering the porous structure of the electrospun mats, a possible explanation is that instead of making the IL denser, the high force enhances the interpenetration between the CEL, IL, and AEL, promoting the effective area of the catalyst.

Fig. 4c and e depict the distinct effects of hot-pressing force in two scenarios: when the CEL, IL, and AEL are hot-pressed together to make a BPM and when they are hot-pressed individually. As shown in Fig. 4c, the perm-selectivity of the BPM slightly increases from 87.0% to 94.4% with the increase in force from 200 kN to 300 kN. Conversely, Fig. 4e reveals no significant perm-selectivity difference when higher forces are employed to hot-press the CEL, IL, and AEL, individually. This is particularly evident for the IL: although Fig. S10 confirms that its thickness and water uptake decrease with increasing force, the perm-selectivity of the IL remains consistent. These results contradict the hypothesis proposed in Section 2.2, that the high pressure directly enhances the perm-selectivity of the IL and thereby improves BPM performance. Instead, the results indicate that high force primarily strengthens the integration between the CEL, IL, and AEL during co-pressing, which enhances BPM perm-selectivity.
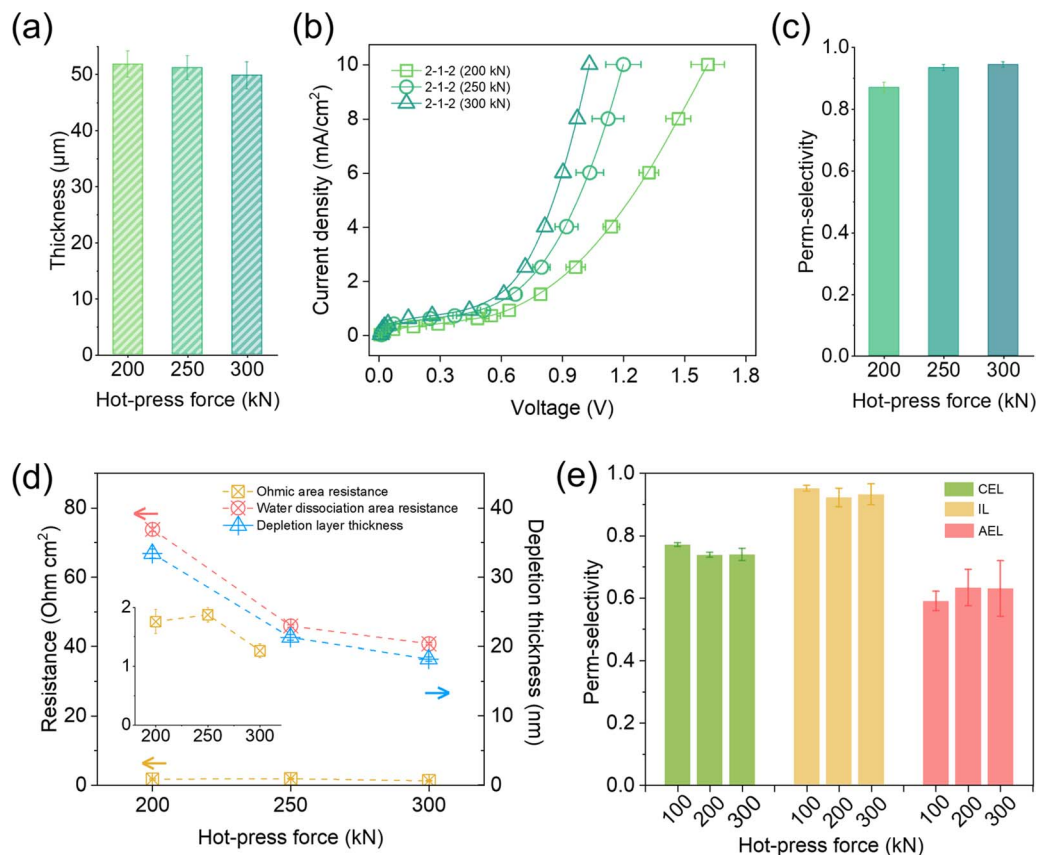
Fig. 4 The effect of hot-pressing force on the performance of the BPM consisting of 2 CELs, 1 IL, and 2 AELs: (a) thicknesses, (b) $i-v$ curves, and (c) perm-selectivities of the BPMs with varying force during hot-pressing; (d) ohmic area resistances, water dissociation resistances, and depletion layer thicknesses of BPMs that are extracted from the EIS Nyquist plots; the inset shows a zoomed-in view of the ohmic area resistance; (e) perm-selectivities of the CEL, IL, and AEL that are hot-pressed individually with varying hot-pressing force.

2.4. Role of the CEL and AEL in water dissociation and perm-selectivity

Although the manipulation of hot-pressing force demonstrates the significance of the integration among the CEL, IL, and AEL in enhancing the water dissociation efficiency and perm-selectivity, the roles of different components in this integration remain unclear. Typically, SPEEK, LbL-coated SPEEK, and FAA-3 electrospun mats are hot-pressed together simultaneously to form a dense BPM (Fig. 5a). To isolate the contribution of the CEL, IL, and AEL to the overall performance of the BPM, we employed a pre-hot-pressing process to hinder the interpenetration between layers. As shown in Fig. 5b, 3 SPEEK electrospun mats were first pre-hot-pressed to form a dense CEL. In the next step, the pre-pressed CELs are stacked together with LbL-coated SPEEK and FAA-3 electrospun mats, and then hot-pressed again. Due to the dense CEL formed in the pre-hot-pressing stage, the integration of this dense CEL into the remaining components can be impeded in the second hot-pressing process. Similarly, as shown in Fig. 5c and d, the pre-hot-pressing process was also applied to LbL-coated SPEEK and FAA-3 electrospun mats, respectively. Because the CEL, IL, or AEL was already densified before the final assembly, its ability to interpenetrate with the other layers was reduced. This

allowed us to isolate and study the contribution of interpenetration from each specific part of the BPM.

Fig. 6a shows the thicknesses of the BPMs featuring different pre-hot-pressed components. Compared to the control membrane, all BPMs containing a pre-hot-pressed component exhibit a slightly higher thickness, indicating that the pre-hot-pressing effectively inhibits the integration of different components. The SEM images in Fig. 5 provide additional evidence: a clear boundary is observable between the pre-hot-pressed electrospun mats and the other components of the BPM. Especially, the delamination of the pre-hot-pressed CEL from the IL can be observed in a dehydrated state in SEM.

As exhibited in Fig. 6b and c, when the CEL was pre-hot-pressed, both the voltage at 10 mA cm^{-2} and the perm-selectivity are comparable to those of the control membrane. This indicates that the interpenetration between the CEL and the IL minimally contributes to the overall performance of the BPM. As shown in Fig. S8, the IL coated with the phytic acid–Fe^{3+} complex remains negatively charged and exhibits a higher perm-selectivity than 4 layers of hot-pressed SPEEK (CEL). Therefore, the hindered interpenetration between the CEL and IL has a limited impact on the perm-selectivity of the BPM. Moreover, as detailed in Section 2.2, the number of SPEEK electrospun mats also has only a minor influence on the thickness of the BPM. As
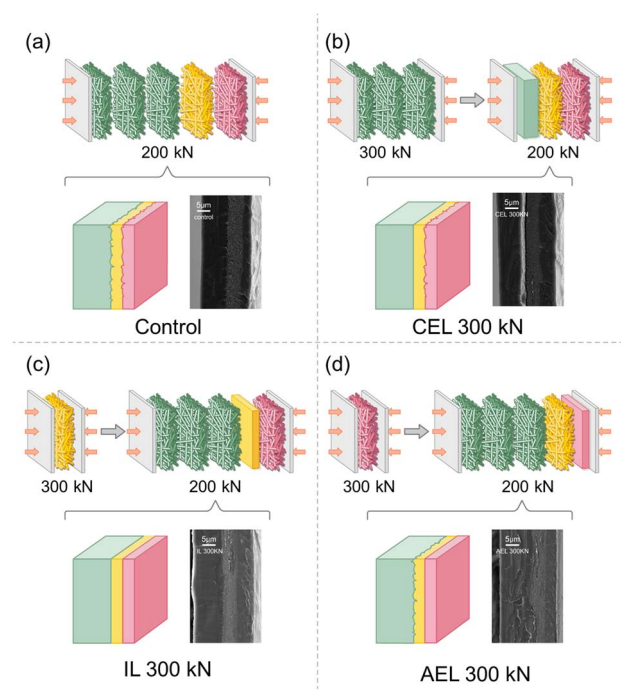
Fig. 5 Method of pre-hot-pressing the CEL, IL, and AEL to investigate their distinct roles in the enhanced BPM performance: (a) control BPM without pre-hot-pressing any parts of BPM; BPMs with a pre-hot-pressed (b) CEL, (c) IL, and (d) AEL.

a result, the ohmic area resistance of the BPM with a pre-hot-pressed CEL also remains the same as that of the control membrane (Fig. 6d). However, compared to the control BPM, both the water dissociation resistance and depletion thickness increase when the CEL is pre-hot-pressed. This can be attributed to the decrease in the effective area of the catalyst due to the restricted interpenetration between the CEL and IL.[21]

Different from the BPM with a pre-hot-pressed CEL, significant increases in voltage at 10 mA cm^{-2} and decreases in perm-selectivity can be observed when the IL or AEL is pre-hot-pressed, emphasizing the more significant role of the interpenetration between the AEL and IL. Due to the thermal crosslinking of the AEL occurring at the pre-hot-pressing temperature (145 °C),[35] pre-hot-pressing the AEL exhibited a more severe negative impact on the interpenetration of the AEL into the IL. Consequently, compared to the BPM with a pre-hot-pressed IL, a greater voltage at 10 mA cm^{-2} and a lower perm-selectivity were observed only when the AEL was pre-hot-pressed. It is worth noting that the first limiting current density of the BPM with a pre-hot-pressed AEL significantly decreases in Fig. 6b. This can be ascribed to the mitigated proton crossover with a pre-hot-pressed AEL, since proton cross-over is more significant than anion crossover.[30] Extracted from the EIS analysis (Fig. S11), Fig. 6d shows that the highest water dissociation resistance is obtained when the IL was pre-hot-pressed, resulting from the decreased effective surface area of the catalyst.[33,34] This confirms the assumption in Section 2.3 that the lower water dissociation resistance obtained at a higher hot-pressing force originates from the enhanced
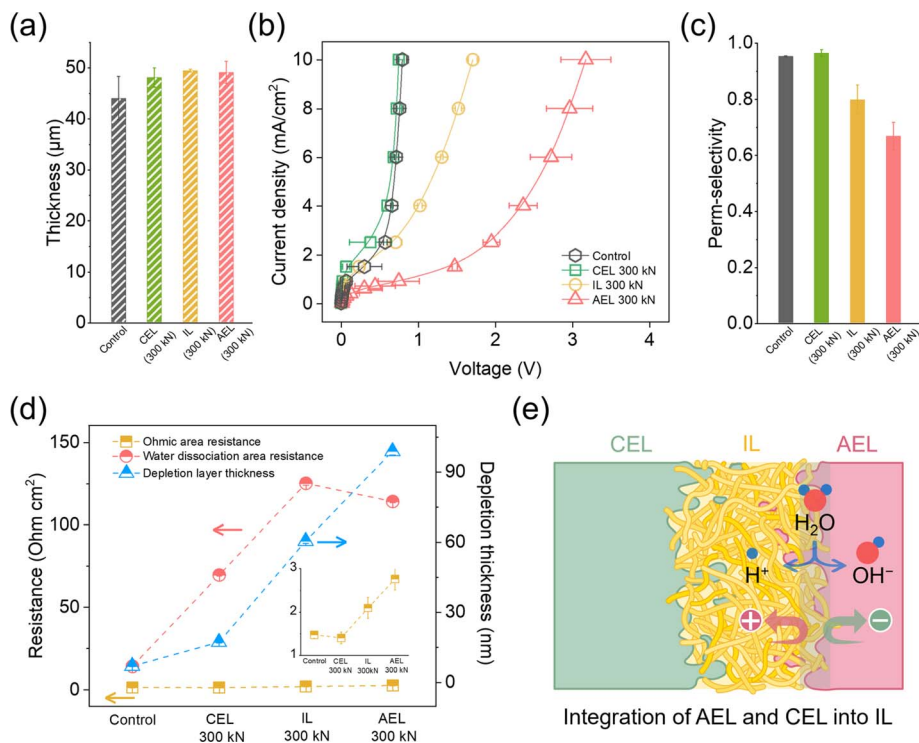

Fig. 6 The performance of BPMs with the pre-hot-pressed CEL, IL, or AEL: (a) thicknesses; (b) i–v curves; (c) perm-selectivities; (d) the ohmic area resistances, water dissociation resistances, and depletion thicknesses; the inset shows a zoomed-in view of the ohmic area resistance; (e) the schematic mechanism of the interpenetration between the CEL, IL, and AEL. The BPM consists of 3 SPEEK electrospun mats as the CEL, 1 phytic acid–Fe^{3+} coated SPEEK mat as the IL, and 1 FAA-3 electrospun mat as the AEL.
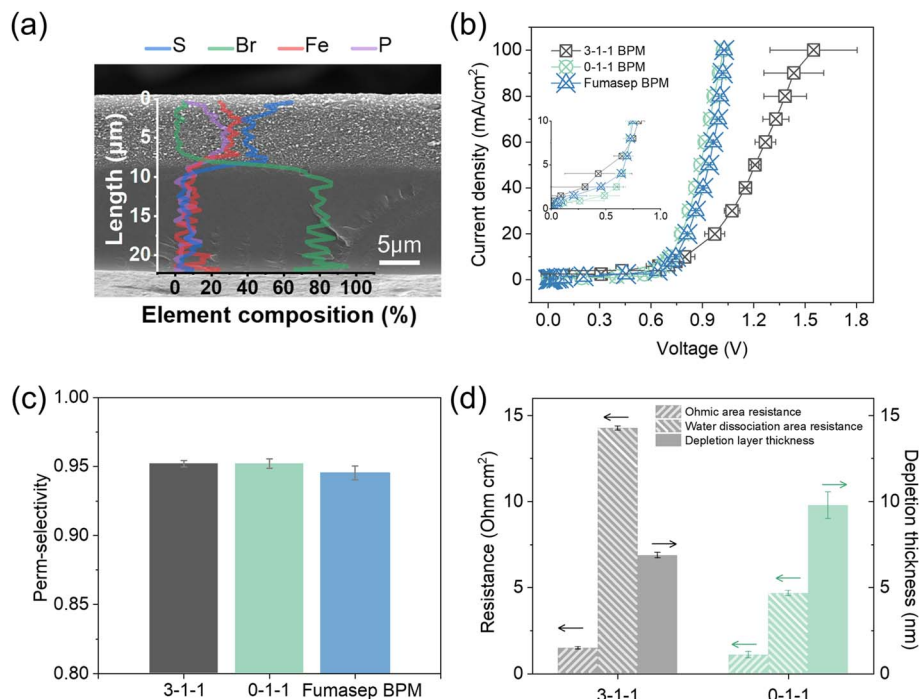
Fig. 7 The performance comparison between the BPM (3−1−1), BPM (0−1−1), and Fumasep BPM: (a) morphology and elemental composition of the cross-section of the BPM (0−1−1) after hot-pressing; (b) $i-v$ curves; the inset presents a zoomed-in view of the $i-v$ curves, focusing on the voltage from 0 to 1 V and current density from 0 to 10 mA cm^2; (c) perm-selectivities; (d) the ohmic area resistances, water dissociation resistances, and depletion layer thicknesses.

interpenetration between the CEL, AEL, and IL, rather than from a denser IL. Meanwhile, it also explains the lower water dissociation resistance observed in Fig. 3c when the thickness of the BPM is lower. Instead of making the IL dense, the enhanced penetration of AEL fibers into the IL creates a more intertwined structure that enhances catalyst accessibility. The schematic mechanism of the CEL, AEL, and IL integration is illustrated in Fig. 6e. Due to the coating of the phytic acid–Fe^{3+} complex on the IL, the IL not only functions as a catalytic layer, but also as a highly selective CEL. In the hot-pressing process, a higher pressure is favored to promote the penetration of the CEL and the AEL into the IL, increasing the surface area for water dissociation. Meanwhile, the boundary formed by the penetration of the AEL into the IL establishes the depletion layer for water dissociation, which is much more important than that formed by the penetration of the CEL into the IL. This mechanism suggests the possibility of integrating only one highly selective, thin, and catalytic IL, and one AEL to make a high-performance BPM that can overcome the trade-off between resistance and perm-selectivity.

2.5. Overcoming the trade-off between resistance and perm-selectivity

Based on the mechanism proposed, a BPM (0–1–1) was prepared by hot-pressing only one IL and one AEL. The cross-section morphology and elemental composition of this BPM are presented in Fig. 7a. When compared with the BPM fabricated by hot-pressing 3 CEL, 1 IL, and 1 AEL (3–1–1), the 0–1–1 BPM not only demonstrates a lower overall resistance, as indicated by the lower

voltage drop at 100 mA cm^{-2} (Fig. 7b), lower ohmic area resistance, and lower water dissociation resistance (Fig. 7d), but also exhibits a higher selectivity, as evidenced by the lower first limiting current density (Fig. 7b) and the higher perm-selectivity (Fig. 7c). It is noteworthy that at 100 mA cm^{-2}, the 3–1–1 BPM has already entered a water transport limitation region, whereas the 0–1–1 BPM has not. This highlights the effectiveness of reducing the thickness of the BPM to enhance the water transport at high current densities.[8,12,13] Moreover, the resistance of the 0–1–1 BPM is comparable to that of a commercial Fumasep BPM at 100 mA cm^{-2}. Significantly, the 0–1–1 BPM exhibits a lower first limiting current density and a higher perm-selectivity, as shown in Fig. 7b and c, respectively. Compared with the reported electrospun BPMs, our 0–1–1 BPM presents a big advantage in both resistance and perm-selectivity (Table S1). This finding emphasizes that leveraging the interpenetration among the CEL, AEL, and IL enables the development of BPMs that not only overcome the trade-off between resistance and selectivity, but also enhance the water transport at high current densities.

3. Conclusions

By manipulating the number of stacked electrospun mats followed by hot-pressing, BPMs with precisely adjustable thicknesses were fabricated. Notably, the BPM with the lowest thickness exhibited the highest perm-selectivity, showing its potential to overcome the trade-off between resistance and selectivity. By varying the force exerted during hot-pressing and the pre-hot-pressed components of the membrane, the

This journal is © The Royal Society of Chemistry 2026

J. Mater. Chem. A, 2026, **14**, 2274–2283 | **2281**

importance of penetration of the AEL into the IL is revealed. This penetration hinders proton crossover, thereby improving the perm-selectivity of the BPM. Inspired by this mechanism, a thin electrospun BPM that integrates one highly selective and catalytic IL and one AEL was produced. This BPM combines low resistance with high perm-selectivity. This work provides informative insights into the structural design of electrospun BPMs that overcome the trade-off between resistance and perm-selectivity. Future work will target the optimization of the catalysts to further enhance the BPM performance and stability.

4. Materials and methods

4.1. Chemicals

Sulfonated poly(ether ether ketone) (SPEEK) with a sulfonation degree of 71% and FAA-3 with an amination degree of 28.3% were purchased from FumaTech GmbH (Germany), and the corresponding chemical structures are shown in Fig. S13. N,N-Dimethylacetamide (DMAC, ReagentPlus, 99%), branched poly(ethylenimine) (PEI, M_w: 750 kDa, 50 wt% in H_2O), phytic acid, iron(III) chloride hexahydrate ($FeCl_3 \cdot 6H_2O$), and hydrochloric acid were purchased from Sigma-Aldrich (Germany). Sodium chloride was supplied by Nouryon (The Netherlands). Demineralized water was obtained from an Elga Water Purification System from Veolia (The Netherlands). All chemicals were used as received.

4.2. BPM fabrication

Negatively charged SPEEK and positively charged FAA-3 were individually electrospun in a wire electrospinner from Elmarco (Czech Republic). The electrospinning conditions are listed in Table S2. SPEEK electrospun mat was chosen as the substrate to embed the catalyst for water dissociation due to its lower swelling ratio in aqueous solution compared to FAA-3.[19] Due to the fragile and soft structure of the electrospun mat, the SPEEK mat was cut into a suitable size and put between plastic meshes to avoid the folding of the electrospun mat during the coating process. Layer-by-Layer (LbL) coating was employed to form a complex of phytic acid and Fe^{3+} on the top of the SPEEK electrospun mat that acts as a catalyst for water dissociation. As shown in Fig. 1a, the SPEEK electrospun mat was first put into a PEI solution (0.1 g L^{-1}, 500 mM NaCl, pH 6) for 15 minutes and subsequently into a phytic acid solution (5 mM, pH 3) and an $FeCl_3$ solution (100 mM) for 15 minutes. In between each coating step, the electrospun mat was rinsed with demi water for 5 minutes to wash away the loosely bound chemicals. The coating of phytic acid and $FeCl_3$ was repeated to form 1.5 bilayers of the phytic acid–Fe^{3+} complex on the SPEEK electrospun mat so that the outmost layer ends with Fe^{3+}.

Hot-pressing was employed to transform porous electrospun mats into a dense ion exchange membrane. As shown in Fig. 1c, the porous electrospun mats of SPEEK, LbL-coated SPEEK, and FAA-3 were cut into 2 cm × 2 cm and stacked accordingly with varying number of layers. Subsequently, the stack was placed between Teflon sheets and hot-pressed together using a LabEcon 300 automated hydraulic laboratory press (Fontijne Presses, The Netherlands) at 150 °C

under a force of 200 kN for 45 minutes. After pressing, the samples were cooled down to 60 °C while maintaining the same pressure. To explore the effects of the thickness of CEL, IL, and AEL, the number of electrospun mats of SPEEK, LbL-coated SPEEK, and FAA-3 was varied. From each BPM, three samples were prepared.

4.3. Characterization and electrochemical measurements

The morphology and the elemental composition of the electrospun mats and BPMs were analysed using a JEOL JSM-IT100 scanning electron microscope (JEOL, The Netherlands). Following the method in our previous study,[19] current density–voltage (i–v) curves under reverse bias (water dissociation) conditions were measured with a six-compartment cell, as depicted in Fig. S14a. 0.5 M Na_2SO_4 and 0.5 M NaCl were employed as the electrolyte rinsing solution and buffer solution, respectively. During the measurement, all the solutions were kept in a thermostatic bath set at 25 °C. The cation and anion exchange membranes from ASTOM Corp. Ltd, (Japan) were used as shielding separators between the compartments. An IVIUM n-stat (IVIUM Technologies BV, The Netherlands) was employed to apply current densities of 0 to 100 mA cm^{-2}, and subsequently measure the voltage drop over the BPM with Haber–Luggin capillaries filled with 2 M NaCl and Ag/AgCl reference electrodes.

To obtain the perm-selectivity of BPMs, the open-circuit voltage (OCV, E_{OCV}) of the BPMs was measured in a two-compartment cell, as depicted in Fig. S14b. 1 L of 0.5 M HCl and 0.5 M NaOH were recirculated on each side. The OCV was monitored for one hour with an IVIUM n-stat (IVIUM Technologies BV, The Netherlands). Based on the Nernst equation, the theoretical open circuit voltage ($E_{theoretical}$) was calculated:

$$E_{\text{theoretical}} = \frac{RT}{F} \ln\left(\frac{[H^+]_{\text{acid}}}{[H^+]_{\text{junction}}}\right) - \frac{RT}{F} \ln\left(\frac{[OH^-]_{\text{junction}}}{[OH^-]_{\text{base}}}\right) \quad (1)$$

where R (8.314 J mol^{-1} K^{-1}), T (298.15 K), and F (96 485 C mol^{-1}) are the gas constant, solution temperature, and Faraday's constant, respectively; $[H^+]_{\text{acid}}$ and $[H^+]_{\text{junction}}$ are the concentrations of protons in the acid compartment and the BPM junction, respectively; $[OH^-]_{\text{acid}}$ and $[OH^-]_{\text{junction}}$ are the concentrations of hydroxides in the base compartment and the BPM junction, respectively. With concentrations of 0.5 M HCl and NaOH, a theoretical OCV of 0.792 V is calculated under the assumption that the concentrations of protons and hydroxides are both 10^{-7} M in the junction of BPM. The perm-selectivity was calculated according to the following equation:[19]

$$\text{Perm-selectivity} = \frac{E_{\text{OCV}}}{E_{\text{theoretical}}} \quad (2)$$

EIS measurements were performed in a six-compartment cell with a SP-300 potentiostat (BioLogic, France). The current density was set at 10 mA cm^{-2} with an amplitude of 10%. The frequency ranged from 10 to 100 kHz with 20 points per decade and 20 measurements per frequency. The resulting EIS data were analyzed using the Z-fit function of EC-Lab software (V11.50).

2282 | J. Mater. Chem. A, 2026, 14, 2274–2283

This journal is © The Royal Society of Chemistry 2026

Author contributions

Tao Wang: conceptualization, methodology, validation, formal analysis, investigation, data curation, writing – original draft. Nadia Boulif: formal analysis, investigation, review & editing. Zandrie Borneman and Kitty Nijmeijer: conceptualization, formal analysis, review & editing, supervision, funding acquisition.

Conflicts of interest

There are no conflicts to declare.

Data availability

The data supporting this article have been included as part of the supplementary information (SI). Supplementary information: including the 14 figures and 2 tables. The data including i–v curves, perm-selectivities, and EIS is presented. See DOI: https://doi.org/10.1039/d5ta08242k.

Acknowledgements

References

1 Z. Yan and T. E. Mallouk, *Acc. Mater. Res.*, 2021, **2**, 1156–1166.
2 M. D. Eisaman, K. Parajuly, A. Tuganov, C. Eldershaw, N. Chang and K. A. Littau, *Energy Environ. Sci.*, 2012, **5**, 7346–7352.
3 P. K. Giesbrecht and M. S. Freund, *Chem. Mater.*, 2020, **32**, 8060–8090.
4 R. Pärnamäe, S. Mareev, V. Nikonenko, S. Melnikov, N. Sheldeshov, V. Zabolotskii, H. V. M. Hamelers and M. Tedesco, *J. Membr. Sci.*, 2021, **617**, 118538.
5 J. C. Bui, E. W. Lees, D. H. Marin, T. N. Stovall, L. Chen, A. Kusoglu, A. C. Nielander, T. F. Jaramillo, S. W. Boettcher, A. T. Bell and A. Z. Weber, *Nat. Chem. Eng.*, 2024, **1**, 45–60.
6 L. Chen, Q. Xu, S. Z. Oener, K. Fabrizio and S. W. Boettcher, *Nat. Commun.*, 2022, **13**, 1–10.
7 M. A. Blommaert, D. Aili, R. A. Tufa, Q. Li, W. A. Smith and D. A. Vermaas, *ACS Energy Lett.*, 2021, **6**, 2539–2548.
8 S. Thiele, B. Mayerhöfer, D. McLaughlin, T. Böhm, M. Hegelheimer and D. Seeberger, *ACS Appl. Energy Mater.*, 2020, **3**, 9635–9644.
9 F. G. Wilhelm, I. Pünt, N. F. A. Van der Vegt, H. Strathmann and M. Wessling, *Ind. Eng. Chem. Res.*, 2002, **41**, 579–586.
10 F. G. Wilhelm, I. Pünt, N. F. A. Van Der Vegt, M. Wessling and H. Strathmann, *J. Membr. Sci.*, 2001, **182**, 13–28.
11 J. J. Krol, M. Jansink, M. Wessling and H. Strathmann, *Sep. Purif. Technol.*, 1998, **14**, 41–52.
12 J. C. Bui, I. Digdaya, C. Xiang, A. T. Bell and A. Z. Weber, *ACS Appl. Mater. Interfaces*, 2020, **12**, 52509–52526.
13 S. Z. Oener, L. P. Twight, G. A. Lindquist and S. W. Boettcher, *ACS Energy Lett.*, 2021, **6**, 1–8.
14 V. Zabolotskii, N. Sheldeshov and S. Melnikov, *J. Appl. Electrochem.*, 2013, **43**, 1117–1129.
15 E. Al-Dhubhani, M. Tedesco, W. M. de Vos and M. Saakes, *ACS Appl. Mater. Interfaces*, 2023, **15**, 45745–45755.
16 D. Kwak, H. M. Tran, D. R. Kandel and J. Lee, *Chem. Eng. J.*, 2025, **507**, 160573.
17 Y. Chen, J. A. Wrubel, W. E. Klein, S. Kabir, W. A. Smith, K. C. Neyerlin and T. G. Deutsch, *ACS Appl. Polym. Mater.*, 2020, **2**, 4559–4569.
18 E. Al-Dhubhani, H. Swart, Z. Borneman, K. Nijmeijer, M. Tedesco, J. W. Post and M. Saakes, *ACS Appl. Energy Mater.*, 2021, **4**, 3724–3736.
19 N. Boulif, M. Houben, Z. Borneman and K. Nijmeijer, *Langmuir*, 2024, **40**, 24795–24807.
20 M. Houben, T. Jansman, Z. Borneman and K. Nijmeijer, *Polymer*, 2024, **307**, 127283.
21 C. Shen, R. Wycisk and P. N. Pintauro, *Energy Environ. Sci.*, 2017, **10**, 1435–1442.
22 E. Al-Dhubhani, J. W. Post, M. Duisembiyev, M. Tedesco and M. Saakes, *ACS Appl. Polym. Mater.*, 2023, **5**, 2533–2541.
23 A. Hohenadel, D. Powers, R. Wycisk, M. Adamski, P. Pintauro and S. Holdcroft, *ACS Appl. Energy Mater.*, 2019, **2**, 6817–6824.
24 J. Balster, S. Srinkantharajah, R. Sumbharaju, I. Pünt, R. G. H. Lammertink, D. F. Stamatialis and M. Wessling, *J. Membr. Sci.*, 2010, **365**, 389–398.
25 G. Cheng, Y. Zhao, W. Li, J. Zhang, X. Wang and C. Dong, *J. Membr. Sci.*, 2019, **589**, 117243.
26 G. Zhang, G. Wang, Y. Liu, H. Liu, J. Qu and J. Li, *J. Am. Chem. Soc.*, 2016, **138**, 14686–14693.
27 S. Z. Oener, M. J. Foster and S. W. Boettcher, *Science*, 2020, **369**, 1099–1103.
28 R. Li, X. Wang, X. Cai, H. Lin, L. Shen, J. Chen, H. Hong and B. Q. Liao, *Sep. Purif. Technol.*, 2018, **197**, 271–280.
29 H. Wang, F. Ding, G. Jin, C. Li and H. Meng, *Colloids Surf., A*, 2017, **520**, 114–120.
30 J. Balster, R. Sumbharaju, S. Srikantharajah, I. Pünt, D. F. Stamatialis, V. Jordan and M. Wessling, *J. Membr. Sci.*, 2007, **287**, 246–256.
31 T. Luo, S. Abdu and M. Wessling, *J. Membr. Sci.*, 2018, **555**, 429–454.
32 M. Tedesco, H. V. M. Hamelers and P. M. Biesheuvel, *J. Membr. Sci.*, 2018, **565**, 480–487.
33 S. Kole, G. Venugopalan, D. Bhattacharya, L. Zhang, J. Cheng, B. Pivovar and C. G. Arges, *J. Mater. Chem. A*, 2021, **9**, 2223–2238.
34 T. Gao, L. Schulte, L. Xiao, E. Yamamoto, A. S. Metlay, C. J. Sheehan, S. Marth, H. Park, S. Sasmal, F. J. Galang, C. Bae, A. Z. Weber, S. W. Boettcher and T. E. Mallouk, *Adv. Energy Mater.*, 2024, **2404285**, 1–10.
35 N. Boulif, Improving membranes for the acid-base flow battery, PhD thesis, Eindhoven University of Technology, 2025.

This journal is © The Royal Society of Chemistry 2026

J. Mater. Chem. A, 2026, **14**, 2274–2283 | **2283**